Study of Crack Propagation in Flat Surfaces Through Experimental and Numerical Work

Ali Jasim Mohammed[1,2], Dr. Abdullah Dhayea[2]

[1]University of Misan, Mechanical Engineering Department, Amarah, Iraq
[2]Department of Mechanical Engineering, University of Baghdad, Iraq
Email: ali_jassim@uomisan.edu.iq

Abstract: This paper aims to numerically model the crack growth path in linear elastic materials under cyclic loading. The effect of crack initiation, propagation, and fatigue life under constant amplitude tensile loading specimens has been studied. The model is preprocessed, the level set updated, the stress intensity factor is calculated, and the crack propagation analysis is performed using Abaqus built-in and external MATLAB functions. Linear elastic fracture mechanics (LEFM) has been adopted for the crack analysis process. The aspects of the implementation and proposed treatments for enriched element processing, framework preparation, stress intensity factor evaluation, and numerical analyses have been described in detail. The proposed method's accuracy and robustness are examined through numerical simulated examples of stationary and crack growth problems using 2D and 3D models. Paris's law has been used to evaluate the fatigue, which involves carefully evaluating stress intensity factors. Different Extended Finite Element Method (XFEM) methodologies and frameworks have been developed to simulate the initiation and propagation of 2 and 3-dimensional micro-cracks through versatile physical models of structures. The results have excellent agreements with the literature's analytical, numerical, and experimental analyses.

Keywords: crack propagation, fatigue loading, XFEM, SIF, crack length, LEFM.

1. Introduction

The Extended Finite Element Method (XFEM) uses a local unit partition to investigate the behavior of materials under different loading conditions and stages. It allows prior knowledge about the solution of the boundary value issue to be added to the approximation approach of the numerical solution by adding enrichment functions, which can be accurately reproduced by the enriched numerical scheme [1][2]. To obtain accurate solutions for crack tip solution stress, the crack proliferation simulation usually requires reshaping the mesh around the crack tip as the crack propagates. The XFEM technique provides a successful methodology for studying crack behavior. Building a mesh on surfaces with cracks is a very delicate and troublesome process. [3]. The XFEM is based on introducing further Degrees Of Freedom (DOFs), which are being in combination with the nodes of the interested elements by the crack geometry. These additional DOFs, associated with some special functions, to get more accurate modeling of micro and macrocracks [4]. This method (XFEM) can enhance the solution of different problems of crack propagation problems [5]. Using XFEM in combination with Linear Elastic Fracture Mechanics (LEFM) to investigate several factors might lead to a slower convergence rate and probably lead to suggestions for some improvements to the fatigue analyses. One of the improvements was the divide of the unit associated with the step function, which represents the displacement discontinuity, and this should have the same order as the FE interpolation of the displacement field. Another improvement is defining the region around the crack tip enrichment regardless of the element size [6]. Under LEFM conditions, the Stress Intensity Factor (SIF) provides a single parameter that describes the stress and strain fields in and outside the vicinity of the crack tip where the plastic region is introduced. The global approach of

fracture compares the material's SIF and the toughness and isothermal fracture in specific areas. The crack initiation and propagation have been studied in different mechanical components such as bearings [7][8] and blades [9]. To determine the initiation and propagation of a crack in a material, the stresses and strains around the crack tip should be sufficient to cause the material to be detached. According to the standards, the defect evaluation analysis is based on a global approach to be applied with fracture mechanics [10]. Based on this technique, the introduced crack has represented a mesh-independent; therefore, the resampling technique is can be declined to describe the crack propagation. Furthermore, the drawbacks of the classical Finite Element Method (FEM) for simulating the propagation of crack, such as the crack propagation shape and the singularity of the node, can be improved by XFEM. This numerical technique uses the standard displacement-based approximation near the crack, which is enriched by integrating the discontinuous and asymptotic fields near the crack tip through the unit partitioning method [11]. In the first, the concept (enriched specific element method) can be applied to all initial formulas with appropriate enrichment for comparison, while in the second stage, is considering the use of concepts borrowed from enrichment [12]. The idea of fracture propagation and its prediction remains a challenging problem due to its dependence on the frequency of impurities and non-homogenous structures within the fractured region. The assessment of the role of these non-homogenous structures on fatigue has been studied by AL-Maliki et al. [13]. A comprehensive implementation of XFEM for single hydraulic fracture propagation has been presented in a previous work of Réthoré et al. [14]. The fracture tip field should be optimized to an adequately capture of the individual approach because, for CFEM simulation, the global mesh should be continuously updated at each step to match the growing fracture geometry [15]. This study aims to predict the spread and growth of cracks by taking two cases from the models and investigating the difference between them and then pointing out the gaps can be occured between them.

Extended finite element method

This research presents the discontinuous enrichment method in a general framework. It is also investigates how the 2D formulation can be have fine meshing for more accurate crack modeling. The concept of modified local enrichment into the FE partitioning of the unit is suggested by Melenk and Babuška [16]. The displacement approximation u(x) in the XFEM is decomposed into a continuous and enrichment part as:

$U(x)=u_{con}(x)+u_{enth}(x)$ (1)

The second part that can be added to Eq. 1 is:

$u^h_{enth}(x) = \sum_{I=1}^{N} N_1(X)(\sum_{a=1}^{M} Fa(x)b_I^a$ (2)

Where: the continuous displacement approximation u_{con} (x) = ∑ N1(x)u1 is the standard approximation in the FEM, and genre (x) is the enrichment part of displacement approximation near the crack (Figure 1). The $N_{I, I}$ = (1, N) are the shape functions of the FE method; however, Fα(x), α = (1, M) are the functions of enrichment, and Check is the vector for the nodal enriched DOF in combination with the elastic asymptotic crack-tip function described by the field of Westergaard.

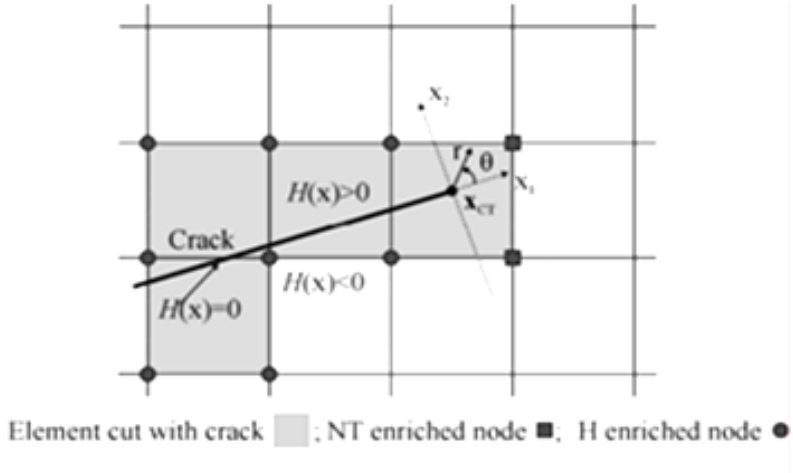

Figure 1. Standard enrichment areas near the crack edges [14].

2. Enrichments

Heaviside Enrichment for Discontinuity

The ability of XFEM to simulate discontinuities stems from applying the Heaviside enrichment function. Various types of Heaviside functions have been proposed in the literature, including:

$$H(\zeta) = \begin{cases} 1 & \forall \zeta > 0 \\ -1 & \forall < 0 \end{cases} \quad (3)$$

Where the value is evaluated of δ(x), the signal distance function is implemented, as shown in point x in the domain of Heaviside after the enrichment process, and x_Γ as with the projection of considered point x onto the slit, it can be defined as:

$$\xi(X) = d.n_x^\Gamma \quad (4)$$

In which

$$d = x - x_\Gamma \quad (5)$$

The unit normal vector of the crack line x_Γ is denoted by x_x^Γ.

By considering the S as the considered set of nodes that have the enrichment functions at the Heaviside, u^{He} it can be represented as:

$$u^{He} = \sum_{i \in S} N_i\ (x) H(\xi) \widehat{a\,i} \quad (6)$$

Enrichment at the edge of the crack

Implementing Enrichment meanings at the crack tip reproduces the vastly nonlinear stress and dislodgment fields around the crack with more accurate results. This process is used due to the variance between the fields' behavior for locations adjacent to sequential cracks and other regions. The standard shape function of FE cannot accurately approximate the fields in both areas. Therefore, because of suitable enrichment at the crack tip, the elements around the crack tip can considerably improve the results obtained in this region. The enrichments can be determined using the nature of these fields. By Considering F as a set of enrichments at the crack tip, yields,

$F=\{f_1, f_2, \ldots f_m\}$ (7)

The crack tip displacement domain can be predicted by.

$$u^{Tip} = \sum_{i \in Tip} N_i(x) \left(\sum_{i \in F} f_{k\,(x)} \widehat{b_{ik}} \right) \quad (8)$$

The Tip is the enriched node using the functions of the enriched elements at the Tip, and $\widehat{b_{ik}}$ are the additional degrees of freedom due to the enrichment. The select tip enrichment functions for uniform materials can be epitomized as follows:

$$F = \sqrt{r}\, sin\left(\frac{\theta}{2}\right), \sqrt{r}\, \text{Cos}(\frac{\theta}{2}), \sqrt{r}\, \sin\frac{\theta}{2} \sin(\theta), \sqrt{r}\, \cos(\frac{\theta}{2}) \sin(\theta)\} \quad (9)$$

Theory

The stress intensity factor (SIF) is the most critical parameter in fracture mechanics. It can be used to investigate whether a crack will propagate in the structure under certain loading conditions. If the stress intensity factor is known, the analytical expressions for the stress and displacement fields at the crack tip location can be solved. The stress component of the plane problem at the crack tip locations is usually given in the polar coordinate system (r, θ). The analytical solution of the stress field of the first plane-type crack at the tip location can be calculated by the Westergaard stress function method [17]. The stress at the crack tip can be shown in Figure 2, and the governing equations will be:

$$\sigma_{xx} = \frac{K_I}{\sqrt{2\pi r}} cos\frac{\theta}{2}\left(1 - sin\frac{\theta}{2} sin\frac{3\theta}{2}\right) \quad (10)$$

$$\sigma_{yy} = \frac{K_I}{\sqrt{2\pi r}} cos\frac{\theta}{2}\left(1 + sin\frac{\theta}{2} sin\frac{3\theta}{2}\right) \quad (11)$$

In the expression above, r and θ are local polar coordinates with the origin at the crack's Tip. When θ is equal to zero at the Tip of the crack, these equations become

$$\sigma_{xx} = \frac{K_I}{\sqrt{2\pi r}} \quad (12)$$

$$\sigma_{yy} = \frac{K_I}{\sqrt{2\pi r}} \quad (13)$$

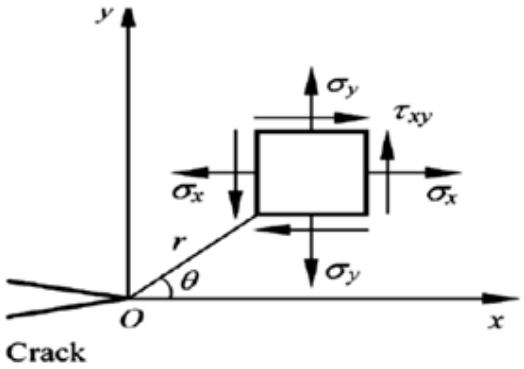

Figure 2. Stress element at the crack tip

Experimental Work

The samples were prepared from steel alloys and designed using the AutoCAD program. The plates were cut according to the dimensions (80*160*4) mm, and the crack lengths were 5, 10 & 15 mm with single central crack and edge crack samples, as seen in Figure 3. The analytical solution for the centrally slotted plates can be found using the following equations [16][18]:

$$K_I = Y\sigma\sqrt{\pi a} \quad (14)$$

$$Y = 1 + 0.256\left(\frac{a}{W}\right) - 1.152\left(\frac{a}{w}\right)^2 + 12.200\left(\frac{a}{w}\right)^3 \quad (15)$$

$$K_n = \sigma\sqrt{\pi a} \quad (16)$$

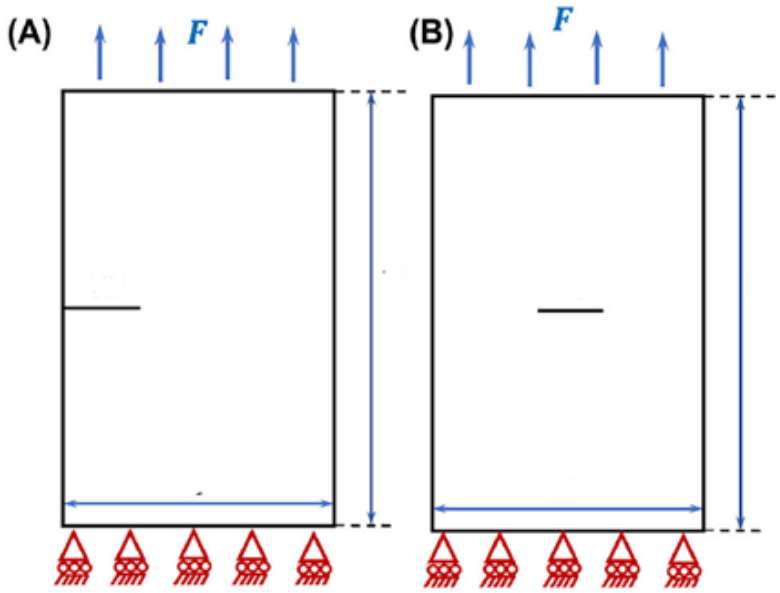

Figure 3. (A) single-edge cracked sample, (B) center cracked sample.

The material used in this work is low-carbon steel 283, which is used in broad fields such as oil tanks, bridges, and many other applications. The first test was the tensile test to determine the mechanical properties. The dog bone test sample shown in Figure 4 was made according to International Standards. A plasma cutting machine has been used to cut the required shapes with additional surface finishing to match the standard requirements.

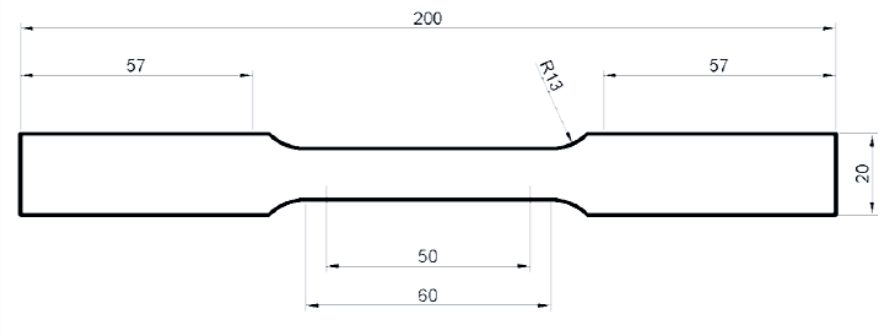

Figure 4. Engineering Drawing By (Auto CAD) for the Designed Tensile Test Specimen

The test samples before and after the test can be seen in Figure 5.

Figure 5. Simple tensile test specimens before the test (LHS) and after the test (RHS).

3. Results and discussions

The load-displacement curve for the test sample was recorded by software linked to the tensile machine. The stress-strain curve was drawn using the gained data, as shown in Figure 6. The mechanical properties of this curve are illustrated in Table 1.

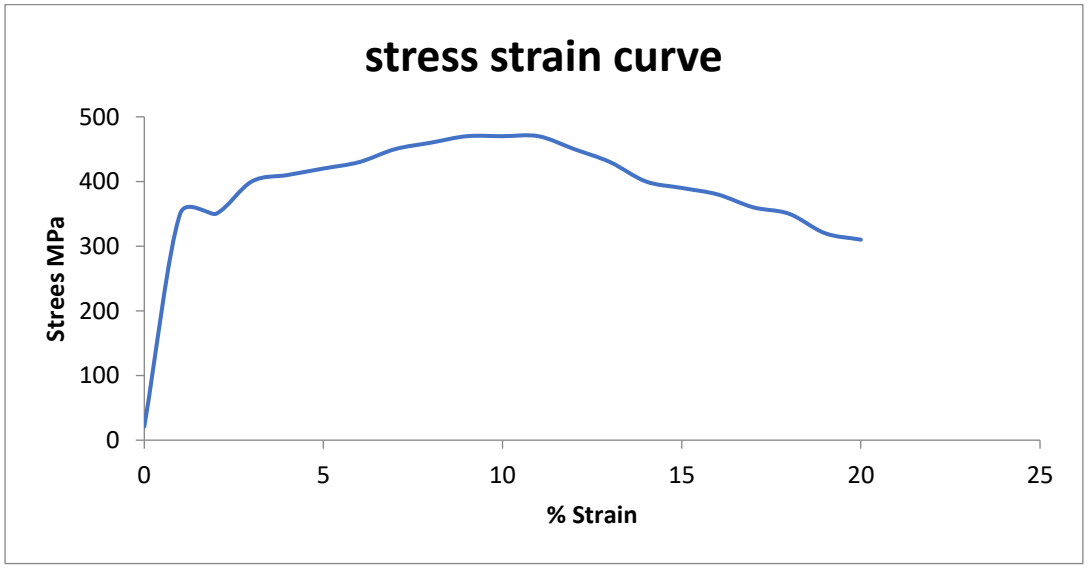

Figure 6. Stress-Strain Curve For Carbone Steel 283

Table 1. The mechanical properties of the tensile test specimen

Thickness mm	Yield stress $\sigma y(MPa)$	Ultimate Stress $\sigma u(MPa)$	Elongation %	Modulus of Elasticity E(GPa)	Poisson's Ratio υ
3	350	472	20	208	0.29

The Chemical Test

This test aims to determine the required chemical compositions of the selected material to ensure the material matches the standard requirements [15]. The chemical compositions of the test material can be seen in Table 2.

Table 2. The Chemical Properties Composition of The Chemical Test Specimen

Thickness (mm)	C%	Si%	Mn%	P%	S%	Fe%
3	0.16	0.19	0.80	0.0075	0.006	Remainder

Numerical Simulation with Its Results

Finite element models and typical mesh generations show the reinforcement plate mesh, as shown in Figure 7 and 8. The mesh type used is square, one of the reinforcement node mesh types for S4R 14460 shell elements and C3D8R 32156 solid elements. XFEM is used in the Abaqus 2020 software version, which allows for the modeling of complex shapes and differs from the traditional method. Boundary conditions and loads can be applied directly to the reference points. For the boundary conditions, the incorporated constraints moving in the direction of the force with the z-axis were only used, constraining all the axes of rotation.

Case1

With the XFEM facilities, the crack propagation simulation has been presented, and the potential of this technique has been revealed. The first case involves taking rectangular panels, as previously mentioned. The dimensions were used in Abaqus software, and the crack lengths were three different. With this software, the crack propagation and the spread of the cracks around the crack tip can be achieved. In this case (case 1), the applied loads were also changed, but the boundary conditions were still the same. In this case, one side is fixed, and the other consists of the applied loads. Figure 7. shows the sample design used in the software and the boundary conditions.

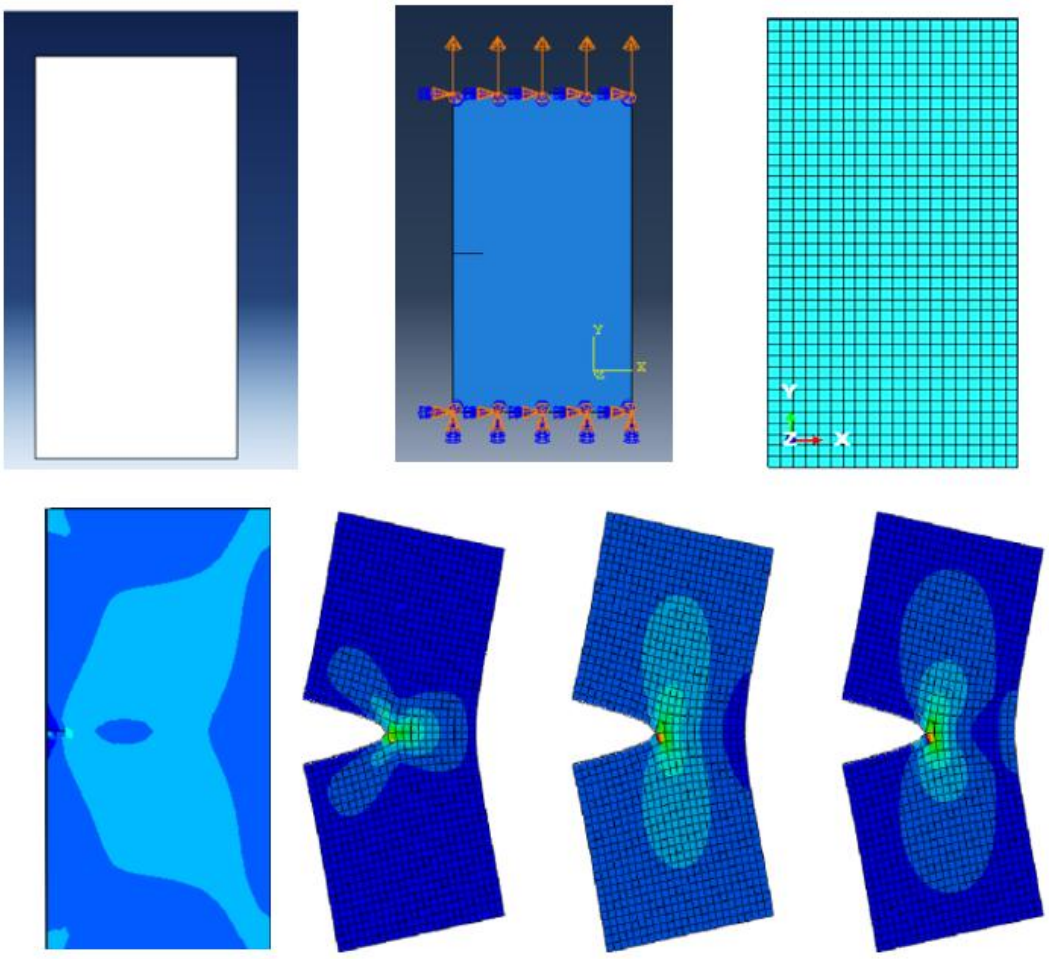

Figure 7. The sample and boundary conditions for the single-edge crack sample.

Looking at the parts of the above figure, the stress distribution around the Tip of the crack can be observed. It is clear that the areas close to the crack cause dispersion in the physical structure of the metal, and the disintegration of its molecules leads to the spread and growth of the crack. It has also been observed that the difference in the crack length affects the speed of its propagation and the change in its path.

Case 2

In the second case, the crack in the middle of the plate is less susceptible to failure because two ends of the sample are exposed to high stresses, leading to different stress distributions. After the collapse, the

material breaks down first at the crack tips. The stress concentration on the edges causes crack propagation in both directions. This reduces the crack spread speed due to carrying the load in two locations instead of one, as shown in Figure 8. The majority of stress concentration and growth are at the crack edge. The first part of the figure in the second row displays the beginning of the crack, the second shows the spread of the crack, and the last presents the occurrence of failure.

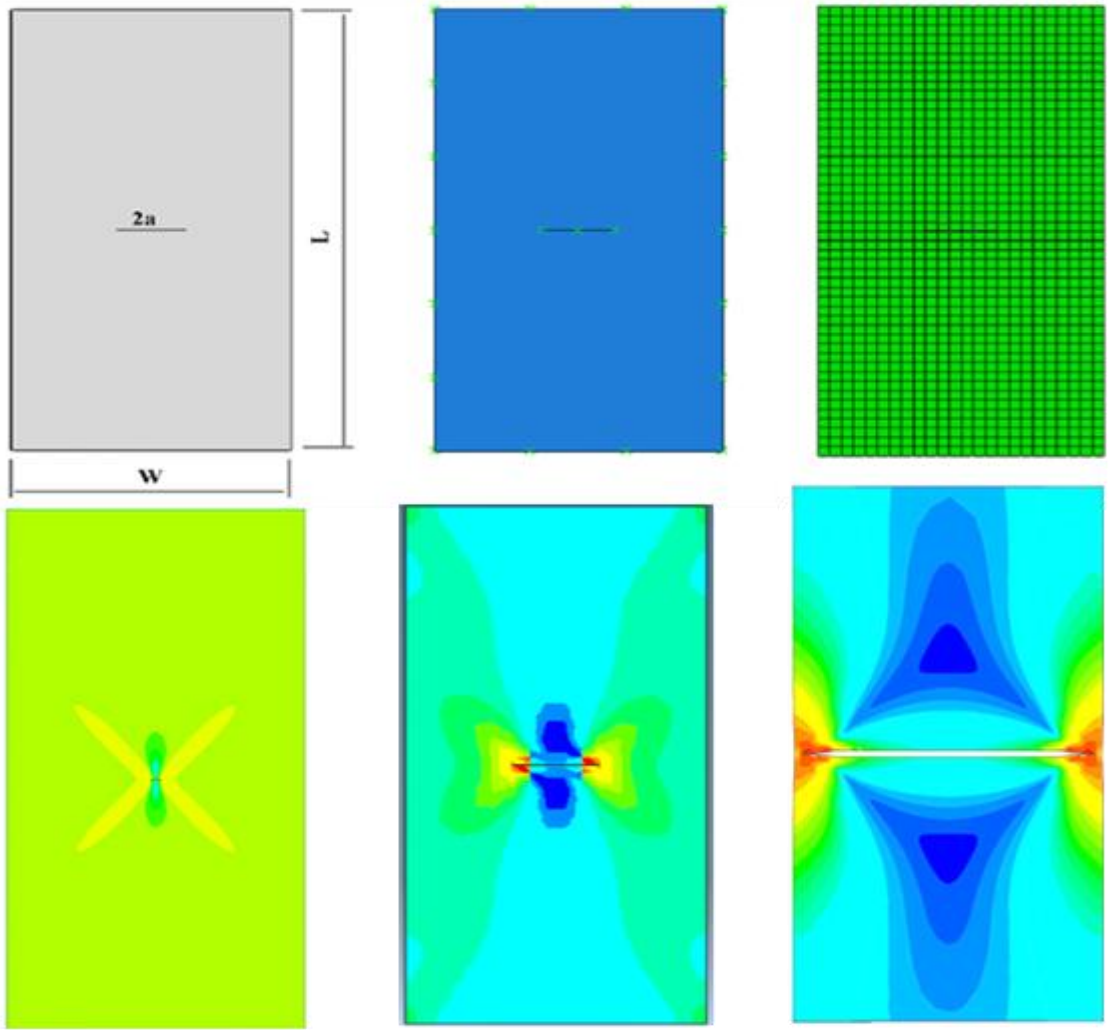

Figure 8. The distribution of von Mises stress under load initiation on different configurations of crack geometry,

Stress Intensity Factor (SIF)

The first test was conducted as an example to calculate the stress intensity factor KI for three different crack lengths of 10 mm, 15 mm, and 20 mm and an element size of 0.589 mm. The results are illustrated in Table 3.

Table 3. Stress Intensity Factor (SIF) KI for various crack lengths and No. of nodes

Number of points taken	a= 10	a=15	a=20
0	35,6	36,8	50,6
1	38,99	40,2	60,1
2	36,3	40,67	65,5
3	36,9	43,5	66,9
4	36,1	41,6	64,3

It is clear from Table 3 that the SIF (K1) can be calculated by extended finite elements, depending on the crack lengths and the element's size.

4. Conclusions

The present study investigated the tensile, flexural, and fracture toughness of a cracked blate made from steel alloys using the XFEM technique. Different crack propagation rates from different models were compared to improve the prediction accuracy, and the causes of varying the SIFs were discussed.

At the critical region, the stress distribution around the crack tip is lower in the centrally cracked specimen than in the side-edge cracked specimen. The modulus of fracture of the central crack was also lower. Therefore, the central crack is less susceptible to failure under fatigue loading than the side-edge cracked specimen. The simulated tensile data were also validated with the experimental results reported in the previous studies. The tensile results were used to check the fracture toughness and SIFs.

Acknowledgments
The authors thank the University of Baghdad and its research centers and laboratories for supporting the completion of this study.

References

[1] X. S. Li et al., "Efficacy and safety of sunitinib in treating metastatic renal cell carcinoma," Chin. Med. J. (Engl)., vol. 124, no. 18, pp. 2920–2924, 2011, doi: 10.3760/cma.j.issn.0366-6999.2011.18.023.

[2] M. Fossati, M. Pagani, S. Miccoli, A. Manes, and M. Giglio, "Numerical calculation of crack parameters for propagation assessment in a complex component with residual stresses," Procedia Eng., vol. 74, pp. 360–367, 2014, doi: 10.1016/j.proeng.2014.06.280.

[3] N. Moës, J. Dolbow, and T. Belytschko, "A finite element method for crack growth without remeshing," Int. J. Numer. Methods Eng., vol. 46, no. 1, pp. 131–150, 1999, doi: 10.1002/(sici)1097-0207(19990910)46:1<131::aid-nme726>3.3.co;2-a.

[4] N. Moës, J. Dolbow, and T. Belytschko, "A finite element method for crack growth without remeshing," Int. J. Numer. Methods Eng., vol. 46, no. 1, pp. 131–150, 1999, doi: 10.1002/(SICI)1097-0207(19990910)46:1<131::AID-NME726>3.0.CO;2-J.

[5] N. Moës, A. Gravouil, and A. Belytschko, "Non-planar {3D} crack growth by the extended finite element and level sets Part I: Mechanical model," Int. J. Numer. Methods Eng., vol. 53, no. 11, pp. 2549–2568, 2002.

[6] J. Remacle, J. Lambrechts, and B. Seny, "Blossom-Quad: A non-uniform quadrilateral mesh generator using a minimum-cost perfect-matching algorithm," International, no. February, pp. 1102–1119, 2012, doi: 10.1002/nme.

[7] T. A. Mankhi, J. H. AL-Bedhany, and S. Legutko, "Investigation of subsurface microcracks causing premature failure in wind turbine gearbox bearings," Results Eng., vol. 16, no. August, 2022, doi: 10.1016/j.rineng.2022.100667.

[8] J. H. I. Al-bedhany, "EFFECT OF COMPRESSION , IMPACT AND SLIPPING ON ROLLING CONTACT FATIGUE AND SUBSURFACE MICROSTRUCTURAL Jasim Hasan Ilik AL-Bedhany," The University of Sheffield, 2020.

[9] C. Navarro, J. Vázquez, and J. Domínguez, "3D vs. 2D fatigue crack initiation and propagation in notched plates," Int. J. Fatigue, vol. 58, pp. 40–46, 2014, doi: 10.1016/j.ijfatigue.2013.02.024.

[10] A. Bousquet, S. Marie, and P. Bompard, "Cleavage crack propagation and arrest in a nuclear pressure vessel steel," Am. Soc. Mech. Eng. Press. Vessel. Pip. Div. PVP, vol. 3, no. Figure 1, pp. 349–358, 2012, doi: 10.1115/PVP2012-78174.

[11] S. K. Kim et al., "Estimation of fatigue crack growth rate for 7% nickel steel under room and cryogenic temperatures using damage-coupled finite element analysis," Metals (Basel)., vol. 5, no. 2, pp. 603–627, 2015, doi: 10.3390/met5020603.

[12] B. Flemisch, A. Fumagalli, and A. Scotti, "A review of the XFEM-based approximation of flow in fractured porous media," SEMA SIMAI Springer Ser., vol. 12, no. 10, pp. 47–76, 2016, doi: 10.1007/978-3-319-41246-7_3.

[13] A. Al-Maliki, J. H. Al-Bedhany, T. A. Mankhi, and S. Legutko, "Assessment of Nonhomogeneous Structures in Steel Contents in Terms of Fatigue Resistance Using Analytical Hierarchy Process," Adv. Sci. Technol. Res. J., vol. 18, no. 1, pp. 334–348, 2024, doi: 10.12913/22998624/182286.

[14] J. Réthoré, R. De Borst, M. Abellan, J. Réthoré, R. De Borst, and M. A. A, "A two-scale approach for fluid flow in fratured porous media To cite this version : HAL Id : hal-00380792," pp. 0–21, 2021.

[15] W. Tian, P. Li, Y. Dong, Z. Lu, and D. Lu, "Numerical simulation of sequential, alternate and modified zipper hydraulic fracturing in horizontal wells using XFEM," J. Pet. Sci. Eng., vol. 183, no. February, p. 106251, 2019, doi: 10.1016/j.petrol.2019.106251.

[16] J. M. Melenk and I. Babuška, "The partition of unity finite element method: Basic theory and applications," Comput. Methods Appl. Mech. Eng., vol. 139, no. 1–4, pp. 289–314, 1996, doi: 10.1016/S0045-7825(96)01087-0.

[17] C. Daux, N. Moës, J. Dolbow, N. Sukumar, and T. Belytschko, "Arbitrary branched and intersecting cracks with the extended finite element method," Int. J. Numer. Methods Eng., vol. 48, no. 12, pp. 1741–1760, 2000, doi: 10.1002/1097-0207(20000830)48:12<1741::AID-NME956>3.0.CO;2-L.

[18] T. L. Anderson, "FRACTURE MECHANICS: Fundamentals and Applications, Fourth Edition," Fract. Mech. Fundam. Appl. Fourth Ed., pp. 1–661, 2017, doi: 10.1201/9781315370293.